ADVANCED OPTICAL MATERIALS
www.advopticalmat.de

Colored, Covert Infrared Display through Hybrid Planar-Plasmonic Cavities

*Joong Hoon Lee, Yeong Jae Kim, Young Jin Yoo, Sehui Chang, Gil Ju Lee, Joo Hwan Ko, Kyung Muk Kang, Debashis Chanda, and Young Min Song**

Artificial covert infrared (IR) displays have recently emerged as an anti-counterfeiting method for spontaneous thermal emissive surfaces and optically encoded information. However, the unnatural appearance of a conventional thermal emissive label in the visible region limits the widespread application of an artificial covert IR display. This paper presents a colored, covert IR display exhibiting visible color patterns and thermally encoded data simultaneously based on a hybrid planar-plasmonic cavity (HPPC). The HPPC is composed of two spectrally distinguished resonant structures: 1) an ultrathin planar cavity with an amorphous silicon (a-Si) layer on gold (Au) for visible coloration and 2) an IR plasmonic cavity with hole-patterned Au on a polymer substrate with a back mirror for thermal data encoding. Such hybridization of multi-band resonance can not only enhance the vivid coloration but also enhance the data storage capacity per unit. Camouflage labels with encrypted thermal data are successfully demonstrated for practical applications using a flexible HPPC. Collectively, the proposed HPPC enables a new type of anti-counterfeiting method that achieves both esthetic, visibly encoded data, and covert, thermally encoded data.

1. Introduction

In modern society, pirated goods have become a global issue as a source of illicit funds for crime organizations.[1] Some countermeasures such as physical anti-counterfeiting technologies have been developed to prevent replication in various forms: watermarks,[2,3] intaglio printing,[4] luminescent ink,[5,6] thermal emissive label,[7–10] and magnetic ink.[11,12] Most importantly, thermal emissive labels using tailored infrared (IR) emissivity implemented using photonic structures have received significant research attention as a promising anti-counterfeiting candidate owing to their facile design and fabrication process for a textured metal surface such as photonic crystal cavities,[13–16] nano-antennas,[17–19] metamaterials,[20–22] and gratings.[23–26] These strategically designed emissive fingerprints are imperceptible to human eyes, and can only be revealed using a thermographic instrument.[27–29]

The key requirement for the universal use of anti-counterfeiting labels such as banknotes, passports, identity cards, tax stamps, and consumer goods is the ability to be blended into the surrounding colored objects (such as camouflage and decoration) while containing multiple encoded information sets.[30–34] Because all of the successful demonstrations of thermal emissive labels reflect their own wavelength of a back reflector, thus not visually harmonious with the colored object, thereby restricting the practical usage. Furthermore, these defined colors are a limitation of extending the tunable band into the visible range for the exponentially increased data capacity. Recently, various multicolored anti-counterfeiting labels have been demonstrated by utilizing light–matter interaction, including metal-ligand coordination,[35,36] plasmonic nanoparticles,[37,38] and metal–insulator–metal resonators.[39–42] However, most existing anti-counterfeiting technologies suffer from a number of defects, such as blurred encrypted data when exposed to chemicals, mechanical instability, and restricted color gamut.[43] Although structural photonic architectures have advantages in terms of high durability, spatial resolution, and non-blurred/fading data compared with organic-based anti-counterfeiting inks, the perfect spectral segmentation for realizing colored anti-counterfeiting is still difficult owing to the resonance crosstalk between visible and IR photonic structures.[44,45]

In this paper, we propose a color, covert IR display with visible and thermally simultaneously encoded data using perfect spectral segmentation based on a hybrid planar-plasmonic cavity (HPPC). The HPPC allows superb spectral segmentation between IR and visible ranges by individually functioning as multi-dimensional resonant structures: 1) a one-dimensionally

J. H. Lee, Dr. Y. J. Yoo, S. Chang, Dr. G. J. Lee, J. H. Ko, K. M. Kang, Prof. Y. M. Song
School of Electrical Engineering and Computer Science
Gwangju Institute of Science and Technology
Gwangju 61005, Republic of Korea
E-mail: ymsong@gist.ac.kr
Dr. Y. J. Kim
Korea Institute of Ceramic Engineering and Technology
Ceramics Test-Bed Center
3321, Gyeongchung-daero, Sindun-myeon
Icheon-si, Gyeonggi-do 17303, Republic of Korea
Prof. D. Chanda
Department of Physics
University of Central Florida
4111 Libra Drive, Physical Sciences Bldg. 430, Orlando, FL 32816, USA
The ORCID identification number(s) for the author(s) of this article can be found under https://doi.org/10.1002/adom.202100429.

DOI: 10.1002/adom.202100429

 © 2021 Wiley-VCH GmbH

stacked sub-100 nm absorbing layer (i.e., amorphous silicon) on gold (i.e., visible range); and 2) a two-dimensionally patterned gold (Au) structure at the micro-scale (i.e., IR range). Although the visible resonant structure is deposited on the IR resonant structure, structural scaling, and dimensional differences enable the independent functioning of the two structures. Theoretical analyses reveal that the visible resonant structure generates various colors depending on the thickness of the amorphous silicon (a-Si) layer, whereas the IR resonant spectrum is dominated by the period, height, and diameter of the cavity. Furthermore, our study theoretically confirmed that structural colorations can be obtained using diverse combinations of different lossy and metallic materials. We successfully fabricated the HPPC based on the optimum spectral design using spectral segmentation. The reflectance measurements from fabricated samples corroborate that the two resonant structures independently function in the spectral region. In addition, we fabricated HPPC labels on the flexible substrate and demonstrated different applications to confirm its capability for practical use. The proposed HPPC can be mass-produced using the wafer-scale fabrication process, which is suitable for various military, anti-counterfeiting, and even heat detection applications.

2. Results and Discussion

2.1. Conceptual Design of a Colored, Covert Infrared Display System

Figure 1a illustrates a schematic of a colored, covert IR display, which consists of an a-Si ultrathin layer coated on a hexagonal micro-patterned plasmonic cavity. The fabricated sample comprises a nanometer-thick a-Si layer with an Au reflector for coloration on top and a hexagonal micro-patterned plasmonic cavity for thermal encoding at the bottom (Figure 1b). Diverse surface colorations can be achieved by modulation of the top a-Si layer thickness, shifting the reflectance dips in the visible region. The optical resonances for multiple colors can be elucidated using a non-trivial phase change (Figure 1c, top). In the IR region, most wavelengths of light are perfectly reflected by the planar metal. However, for long-wave infrared (LWIR) covert information, the IR reflectance on the bottom side should be designed in the far-IR region (from 8 to 14 wavelength ranges) with a hexagonal micro-patterned array (Figure 1c, bottom). The perforated structure of the HPPC acts as a subwavelength diameter aperture to generate extraordinary light transmission (EOT), and the

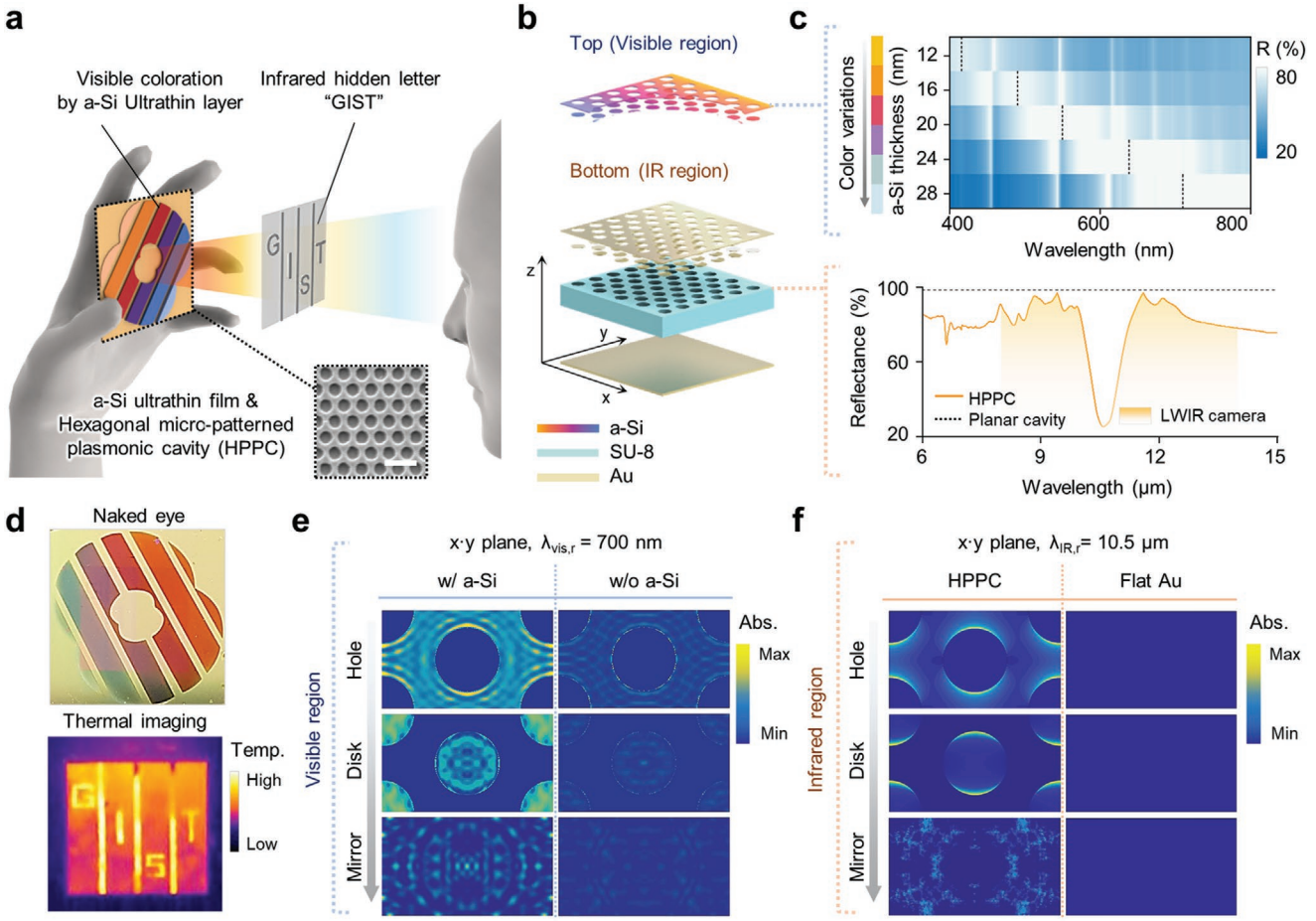

Figure 1. a) Concept illustration of hybrid planar-plasmonic cavities (HPPC) with top-view SEM images (inset). b) Illustration of an exploded view of the HPPC. c) Optical spectra of the top and bottom structures in the visible and infrared regions. d) Photograph (top) and thermal image (bottom) of the HPPC sample. e) Absorption profiles of the HPPC with a-Si (left) and without a-Si (right) at 700 nm wavelength. f) Absorption profiles of the HPPC and planar cavity at 10.5 μm wavelength.

© 2021 Wiley-VCH GmbH

transmitted light is sequentially coupled to Fabry–Pérot cavity modes. A highly selective IR spectrum is feasible by achieving coherence between the EOT and the Fabry–Pérot effect.[46] We demonstrate colored/infrared encoding images using a combination of an a-Si/Au colored layer and a hexagonal micro-patterned cavity. The colored symbol is completely distinguished, unlike the IR encoded image "GIST", which is concealed from the naked eye. The a-Si ultrathin layers with different thicknesses were deposited on the designated area of the symbol to verify the color variation (Figure S1, Supporting Information, for the optical microscope images). Furthermore, the "GIST" letters are patterned at the center of the colored symbol, which can only be detected using an LWIR thermal camera (Figure 1d; Movie S1 and Figure S2, Supporting Information, for structural design). To observe the enhanced absorptance for coloration/infrared emissivity in the HPPC, we calculated the absorption profile (Figure 1e,f). Enhanced absorption is observed in the visible region at the a-Si/Au interface at the resonant wavelength = 700 nm (Figure 1e, left); however, a considerably low intensity is observed in the sample without the a-Si layer (Figure 1e, right). Electromagnetic waves are detected in the IR region at the resonant wavelength, =10.5 µm at the edge of the hexagonal micro-patterned holes (Figure 1f, left), whereas the absorptance is negligible in the planar metal surface, which behaves as a perfect mirror (Figure 1f, right).

2.2. Material Combinations and Geometrical Dependency

Figure 2a illustrates the configuration of an ultrathin a-Si-coated top Au layer for optical simulation. The a-Si material was selected for coloration owing to its absorption property in the visible spectrum. The reflectance dips decrease as the top metal layer thickness increases at a specific wavelength (Figure 2b, top). The interface reflection between the highly absorbing media and the top metal reflector facilitates strong resonance based on a non-trivial phase change.[47,48] In addition, the top metal layer thickness critically affects color saturation (Figure 2b, bottom). The color saturation values dramatically decreased below the 30 nm thickness of the top metal reflector (see Figure S3, Supporting Information for details). Figure 2c shows the color representations according to various material combinations and the change in the top absorbing layer thickness from 0 to 50 nm. The candidate optical coating material for coloration should be highly absorbable at visible wavelengths. Chromaticity plots display the calculated reflectance results of material combinations in the standard red, green, and blue (sRGB) gamut on the International Commission on Illumination (CIE) color space (see Figure 2d, Figure S4, Supporting Information for details). Figure 2e illustrates the configuration of micro-patterned arrays in the IR spectrum to demonstrate geometrical dependency, and the structural parameters are set as follows: cavity thickness t_c, diameter d, depth h, and period p. Figure 2f shows the EOT of the hexagonal micro-patterned Au array without the bottom mirror (Figure 2f, top). Compared with the non-patterned Au surface (i.e., flat Au), induced transmission of light occurs through the structure with regularly repeated patterns on the subwavelength scale. Furthermore, the reflectance dip shifts along the cavity thickness variation (Figure 2f, bottom). The multispectral property caused by the Fabry–Pérot resonance occurs in the plasmonic cavity depending on the cavity thickness (Figure 2g). Moreover,

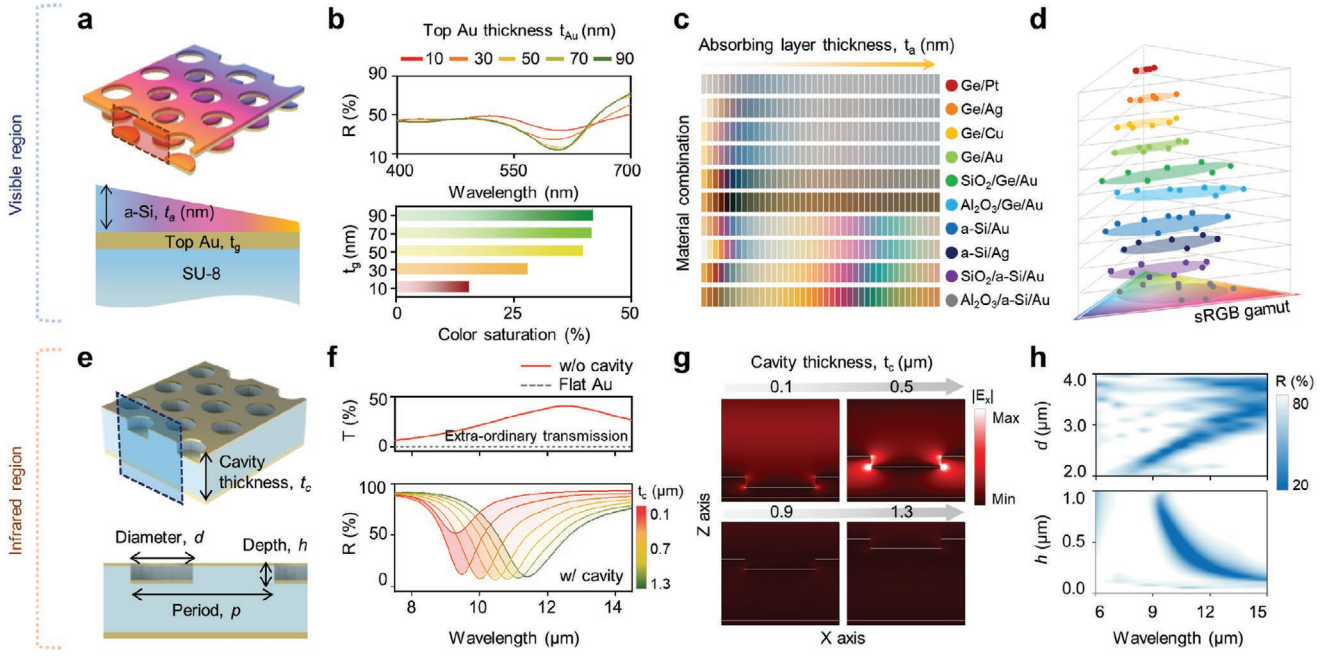

Figure 2. a) Concept illustration of the top a-Si and Au layers. b) Reflectance and color saturation plots of HPPC depending on the top Au thicknesses. c) Color representation of diverse combinations of materials. d) Color gamut from Figure 2c. e) Schematic illustration of HPPC. f) Comparison of the transmittance plots of HPPC with hole/disk cavity and flat Au (top), reflectance of HPPC depending on the cavity thickness (bottom). g) E-field profiles of HPPC depending on the cavity thickness. h) Contour plots of reflectance spectra depending on the diameter and height of hole/disk.

© 2021 Wiley-VCH GmbH

contour plots of the reflectance as a function of the hole/disk d and h were calculated. Because the subwavelength hole/disk diameter determines the light transmission, sharp dips in the IR reflectance are red-shifted as the hole/disk diameter increases (Figure 2h, top). As h of the HPPC increases, the transmitted light exhibits high spectral selectivity with hybridization between the EOT and the Fabry–Pérot resonance. In contrast, when h decreases, light coupling between the hole disks weakens because of the lowered transmittance of the micro-patterned Au layer (Figure 2h, bottom).[46]

2.3. Encryption/Characterization of the Colored, Covert Infrared Display System

The fabrication process of the colored, covert IR display is shown in **Figure 3**a. The fabrication process as follows: 1) An Au back reflector (≈150 nm thickness) was deposited on a silicon substrate using an e-beam evaporator. 2) SU-8 was spin-coated on the Au back reflector with a thickness of 1.1 µm, and then prebaked at 95 °C for 1 min. Next, the samples were treated with UV exposure (1 min) and post-exposure baked (95 °C for 1 min) to the cavity spacer. 3) A 2D lateral micro-pattern was formed using a conventional photolithography process. The positive photoresist (AZ 5214) is used to form the etch mask. 4) Anisotropic etching was performed at a height of 600 nm using reactive ion etching (RIE). The selectivity between the positive photoresist and SU-8 was nearly 1:1, which was successfully employed as an etch mask instead of metal etch mask.[49] 5) After etching process, the top Au layer has evaporated onto a hexagonal patterned cavity that consist of Au/Su-8/Au. 6) We deposited an a-Si layer with thickness modulation (i.e., from 12 to 28 nm in 4 nm steps) sequentially (see Section 4 for details). The fabricated samples were captured using scanning electron microscopy (SEM) to determine geometric information (Figure 3b, tilt view, left; cross section, right). The visible and IR spectra of the surfaces are plotted as shown in Figure 3c,e, respectively for quantitative analysis and confirmation of mutual non-interference in each domain. The reflection spectra of all the fabricated samples in the visible region were measured using a UV–vis–NIR spectrometer. The dip position shifted toward longer wavelengths as the a-Si layer thickness increases (see Figure S5, Supporting Information for details). Figure 3d shows colored samples with different a-Si thicknesses based on these quantitative analyses. To estimate the angle dependence of the visible region, we calculated the diffraction efficiencies using the numerical simulations shown in Figure S6, Supporting Information, for diffraction robustness. The result shows that the diffraction efficiency is dominated with filling fraction. The high-order diffraction can be controlled at the filling fraction under 50% (i.e., low diffraction efficiency). The samples were fabricated at a filling fraction of 50% based on the calculation results to maintain a low diffraction in the entire visible region (see Figure S7, Supporting Information for experimental results). The IR reflectance spectra of the samples were measured using a Fourier transform infrared spectrometer (FTIR) coupled with a 15× microscope (Figure 3e). Because all theoretical simulations are performed in the case of normal incidence, a customized square-shaped slit was adopted to compensate for the optical effect of the high numerical aperture (0.4) of the objective lens. The dip positions of the samples exhibit excellent uniformity regardless of the top dielectric layer thickness (i.e., the difference in chromatic coloration). Furthermore, Figure 3f shows the thermal image of the samples using a commercial thermal camera (spectral range of 7.5–14 µm) as an analyzer, representing the distinct IR characteristics of the HPPC. The dotted lines indicate the fabricated HPPC area. With the resonances of the HPPC layer at LWIR, the absorption light exhibits distinct temperatures corresponding to the sensitivity spectrum of the analyzer, which is clearly distinguished from the external area.

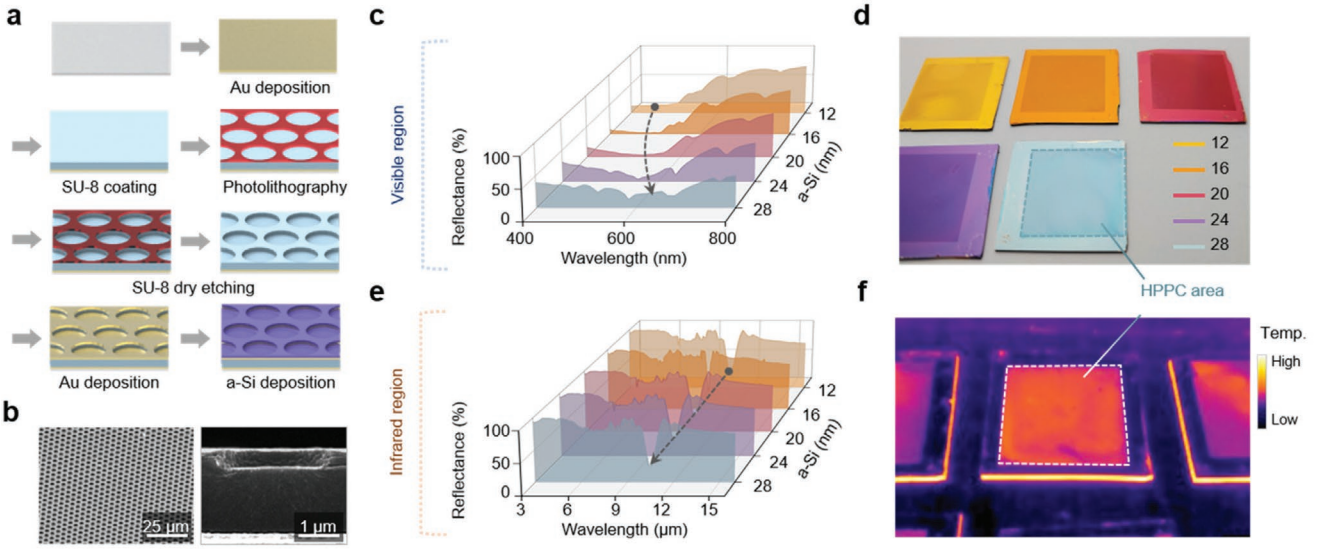

Figure 3. a) Fabrication process of a colored, covert infrared display. b) Top (left) and cross-section views (right) of SEM images of the fabricated HPPC sample. c) Reflectance spectra of the HPPC in the visible spectral regions. d) Photographs of colored HPPC samples with different a-Si thicknesses. e) Reflectance spectra of the HPPC in the infrared spectral regions. f) Thermal image of colored HPPC samples with different a-Si thicknesses.

© 2021 Wiley-VCH GmbH

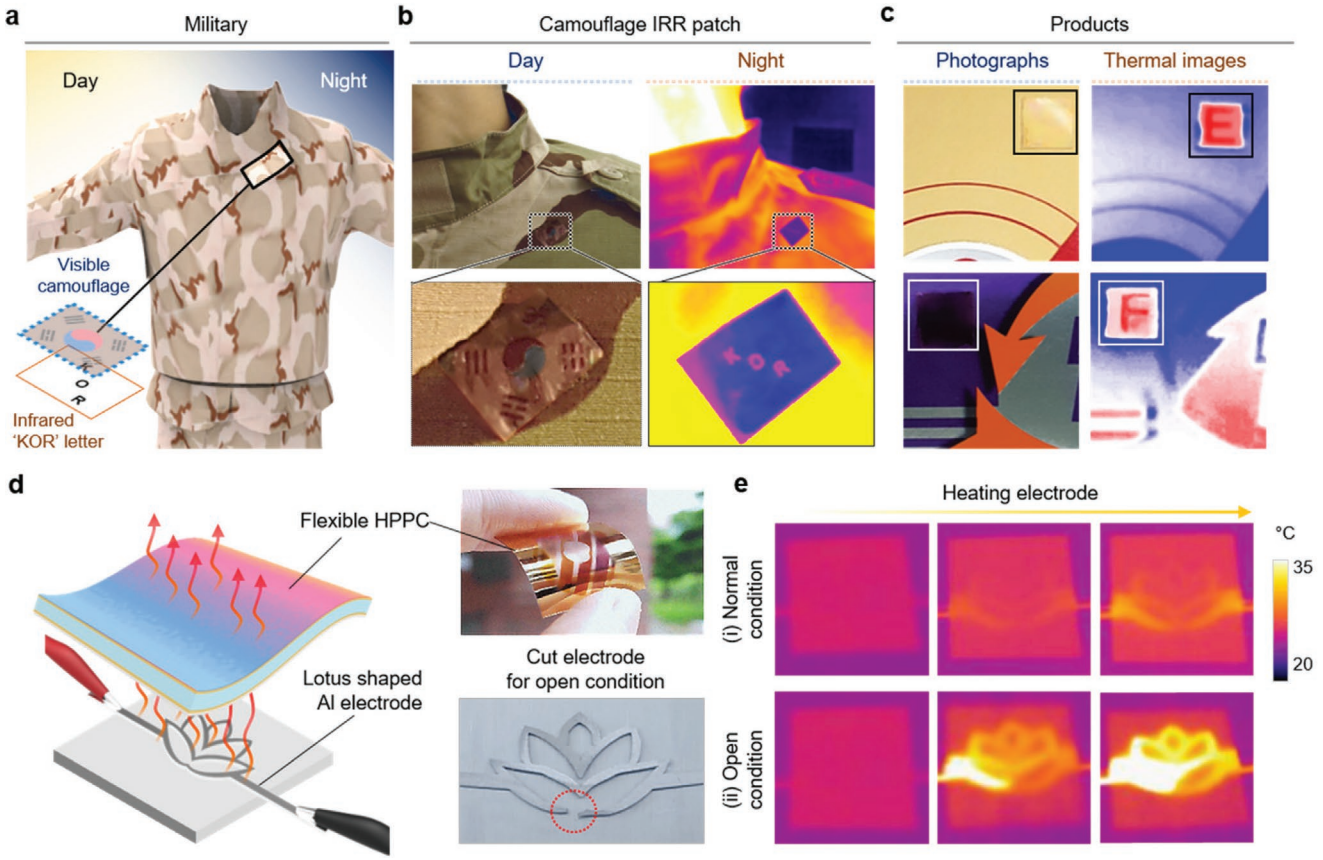

Figure 4. a) Schematic illustration of a camouflage HPPC label. b) Photographs of the fabricated IR/IFF HPPC patch in the visible region (day) and infrared region (night). c) Camouflage HPPC labels on a commercial product as an anti-counterfeiting label. d) Schematic illustration of thermal emissive features with a heated lotus-shaped electrode. e) Thermal images in normal and open conditions.

To demonstrate its practical applications, we fabricated an infrared/identification friend or foe (IR/IFF) patch using a camouflage HPPC label (**Figure 4**a). For the visible camouflage, the national flag of South Korea is displayed at the top a-Si and Au layer of the HPPC and the letters "KOR" are encoded as infrared data for peer identification in the night environment, as clearly shown in the thermal images in Figure 4b. Unlike conventional IR/IFF patches, the fabricated IR/IFF HPPC patch can strengthen the security level by encoding specific data in the IR region that is distinct from the optical data in the visible region. In addition, the visible camouflage HPPC label can also be employed as an anti-counterfeiting method for commercial products (Figure 4c). The flexibility and esthetic features of HPPC ensure that the camouflage HPPC label provides a high degree of freedom in design and utilization. In addition, the fabricated HPPC can be extended for heat detection of electrodes by enhancing the heat radiation. The lotus-shaped metal in Figure 4d is used as an electrode in the HPPC sample to demonstrate local heat detection. Lotus-shaped heat emission is observed as the temperature of the electrode increases (Figure 4e). In the open condition, the bottom side of the lotus electrode was cut, and it exhibited an extremely high temperature due to current flow (Figure 4e, bottom-right). The HPPC can be applied as a heat detection label, providing not only enhanced heat radiation but also esthetic features.

3. Conclusion

In this paper, we presented a colored, covert infrared display with spectrally segmented features based on an HPPC for anti-counterfeiting applications. The proposed colored, covert IR display realizes not only colorful appearances, but also infrared encoded information. In addition, HPPC provides camouflage compatibility with a wide range of products and also increased information capacity through its multicolored property. Spectral analyses of the individual photonic structures of the HPPC indicate that optical and thermal resonances can be induced using the thickness of the a-Si and the height/diameter/period of the plasmonic cavity, respectively. The colored/infrared images of the HPPC were successfully fabricated by optimizing the geometrical parameters. Moreover, we theoretically confirmed that structural colorations can be obtained using diverse combinations of different lossy and metallic materials. The reflectance spectra and thermal/optical imaging of the fabricated samples corroborate that the two resonant structures independently function in the spectral region. Last, the camouflage HPPC label demonstrated its capability for practical use in different applications such as military security, anti-counterfeiting, and heat detection. The proposed HPPC can be extended to develop the multimodal anti-counterfeit system in combination with novel materials, which have polarization or phase transition properties.

© 2021 Wiley-VCH GmbH

4. Experimental Section

Optical Calculation: The rigorous coupled-wave analysis (RCWA) method was performed to calculate the reflectance and absorption of the HPPC using commercial software (DiffractMOD, RSoft Design Group, USA). The second diffraction order and a grid size of 0.1 nm^2 were set in the RCWA during the optical calculation to numerically stabilize the results. The material dispersions and extinction coefficients were considered during the entire calculation process. MATLAB software (Mathworks, USA) was also used to calculate both the effective complex refractive indices based on the volume average theory and chromatic information from the reflectance.[50]

Optical Characterization: The reflectance spectra of the fabricated samples in the visible region were measured using a UV–vis–NIR spectrometer (Cary 500, Varian, USA) at normal incidence with a tungsten-halogen lamp as the source. In the LWIR domain, a FTIR spectrometer (Vertex 70v, Bruker, USA) was coupled with an optical microscope unit (Hyperion 1000, Bruker, USA) at room temperature. A germanium objective lens (15×, NA = 0.4) was mounted on the microscope, and all measurements were calibrated using Au as a standard. The infrared images were recorded using an uncooled VOx micro-bolometer camera (FLIR E5-XT, FLIR, USA). To improve the resolution, a customized lens was mounted with a thermal camera.

Deposition of Colored, Covert IR Display: For rigid samples, single-side polished silicon wafers (100, n-doped, electric resistivity = 1^{-30} Ω cm) were generally selected as the substrate and treated with a buffered oxide etchant for 3 min to remove the native oxide layer. Subsequently, the substrate was sonicated in acetone, methanol, and deionized (DI) water for 5 min. For flexible samples, a commercial 2.5 μm polyester thin-film (SpectroMembrane, Chemplex Industries, Inc., Palm City, USA) was used. All the materials (Au, a-Si) were deposited using electron beam evaporation (KVE-E2000, Korea Vacuum Tech Ltd, Korea) under high vacuum (≈10^{-6} Torr) at a rate of ≈2 Å s^{-1}, ≈1 Å s^{-1}, and ≈1 Å s^{-1}, respectively. The Au film was deposited to a thickness of 150 nm, which is sufficient to form a metal reflector. A 5 nm (Ti) layer was adopted as an adhesive layer between the Au film and the substrate. The 50-nm-thick top Au films were deposited under the same condition as the Au back mirror. Thus, the a-Si layer was deposited with the desired thickness.

Encryption of Colored, Covert IR Display: Photolithography was used with a positive photoresist (AZ 5214, AZ Electronic Materials, Luxembourg) as an etch-mask for encoding the designed optical information (letter and logo) with covert characteristics in the LWIR. In the lithography process, a mask aligner (MJB3 UV400, Karl Suss, Germany) was used with a patterned photomask. In each patterned region, the anisotropic etching process was performed at a height of 600 nm using the RIE process (Oxford Plasmalab 133, Oxford Instruments, UK). After performing the etching process, the remaining photoresist was gently removed to reveal the patterned area.

Supporting Information

Supporting Information is available from the Wiley Online Library or from the author.

Acknowledgements

J.H.L. and Y.J.K. contributed equally to this work. This research was supported by the National Research Foundation of Korea (NRF), funded by the Korean government (NRF-2018R1A4A1025623 and NRF-2020R1A2C2004983), the Korean Institute of Energy Technology Evaluation and Planning (KETEP) and the Ministry of Trade, Industry & Energy (MOTIE) of the Republic of Korea (No. 20183010014310), and by the GIST Research Institute (GRI) through a grant funded by the GIST in 2020. This work was also supported by the Institute of Information & Communications Technology Planning & Evaluation (IITP) through a grant funded by the Korean government (MSIT) (No. 2020-0-01000, light field and LiDAR sensor fusion systems for full self-driving).

Conflict of Interest

The authors declare no conflict of interest.

Data Availability Statement

The data that support the findings of this study are available from the corresponding author upon reasonable request.

Keywords

anti-counterfeiting, camouflage, covert display, infrared emitters, structural coloration

Received: February 28, 2021
Revised: May 3, 2021
Published online:

[1] E. L. Prime, D. H. Solomon, *Angew. Chem. Int. Ed.* **2010**, *49*, 3726.
[2] M. Li, X. Yuan, H. Chen, J. Li, *IEEE Access* **2020**, *8*, 72308.
[3] S. Huang, J. K. Wu, *IEEE Trans. Inf. Forensics Secur.* **2007**, *2*, 164.
[4] C.-F. Wang, R. Cheng, W.-Q. Ji, K. Ma, L. Ling, S. Chen, *ACS Appl. Mater. Interfaces* **2018**, *10*, 39205.
[5] H. Kang, J. W. Lee, Y. Nam, *ACS Appl. Mater. Interfaces* **2018**, *10*, 6764.
[6] Z. Gao, Y. Han, F. Wang, *Nat. Commun.* **2018**, *9*, 3977.
[7] D. Franklin, S. Modak, A. Vázquez-Guardado, A. Safaei, D. Chanda, *Light: Sci. Appl.* **2018**, *7*, 93.
[8] G. Bakan, S. Ayas, M. Serhatlioglu, C. Elbuken, A. Dana, *Adv. Opt. Mater.* **2018**, *6*, 1800613.
[9] S. Chandra, D. Franklin, J. Cozart, A. Safaei, D. Chanda, *ACS Photonics* **2018**, *5*, 4513.
[10] G. J. Lee, Y. J. Kim, H. Y. Kim, Y. J. Yoo, Y. M. Song, *Adv. Opt. Mater.* **2018**, *6*, 1800707.
[11] R. Arppe, T. J. Sorensen, *Nat. Rev. Chem.* **2017**, *1*, 31.
[12] B. Song, H. Wang, Y. Zhong, B. Chu, Y. Su, Y. He, *Nanoscale* **2018**, *10*, 1617.
[13] S. Y. Lin, J. Moreno, J. G. Fleming, *Appl. Phys. Lett.* **2003**, *83*, 380.
[14] R. J. Shiue, Y. Gao, C. Tan, C. Peng, J. Zheng, D. K. Efetov, Y. D. Kim, J. Hone, D. Englund, *Nat. Commun.* **2019**, *10*, 109.
[15] H. Xing, J. Li, Y. Shi, J. Guo, J. Wei, *ACS Appl. Mater. Interfaces* **2016**, *8*, 9440.
[16] X. Fei, T. Lu, J. Ma, S. Zhu, D. Zhang, *Nanoscale* **2017**, *9*, 12969.
[17] E. Sakat, L. Wojszvzyk, J.-P. Hugonin, M. Besbes, C. Sauvan, J.-J. Greffet, *Optica* **2018**, *5*, 175.
[18] M. D. Wissert, K. S. Ilin, M. Siegel, U. Lemmer, H.-J. Eisler, *Nano Lett.* **2010**, *10*, 4161.
[19] F. Neubrech, D. Weber, J. Katzmann, C. Huck, A. Toma, E. D. Fabrizio, A. Pucci, T. Hartling, *ACS Nano* **2012**, *6*, 7326.
[20] J. Jang, T. Badloe, Y. Yang, T. Lee, J. Mun, J. Rho, *ACS Nano* **2020**, *14*, 15317.
[21] J. Jang, T. Badloe, T. C. Sim, Y. Yang, J. Mun, T. Lee, Y.-H. Cho, J. Rho, *Nanoscale* **2020**, *12*, 21392.
[22] Z. J. Coppens, J. G. Valentine, *Adv. Mater.* **2017**, *29*, 1701275.
[23] A. K. Pandey, A. K. Sharma, C. Marques, *Plasmonics* **2020**, *16*, 9.

© 2021 Wiley-VCH GmbH

[24] Y. Wang, I. Aravind, Z. Cai, L. Shen, G. N. Gibson, J. Chen, B. Wang, H. Shi, B. Song, E. Guignon, N. C. Cady, W. D. Page, A. Pilar, S. B. Cronin, *ACS Appl. Mater. Interfaces* **2020**, *12*, 17459.
[25] G. J. Lee, D. H. Kim, S.-Y. Heo, Y. M. Song, *ACS Appl. Mater. Interfaces* **2020**, *12*, 53206.
[26] S. Y. Heo, G. J. Lee, D. H. Kim, Y. J. Kim, S. Ishii, M. S. Kim, T. J. Seok, B. J. Lee, H. Lee, Y. M. Song, *Sci. Adv.* **2020**, *6*, eabb1906.
[27] R. J. H. Ng, R. V. Krishnan, H. Wang, J. K. W. Yang, *Nanophotonics* **2020**, *9*, 533.
[28] A. Tittl, A.-K. U. Michel, M. Schäferling, X. Yin, B. Gholipour, L. Cui, M. Wuttig, T. Taubner, F. Neubrech, H. Giessen, *Adv. Mater.* **2015**, *27*, 4597.
[29] Z. Xu, Q. Li, K. Du, S. Long, Y. Yang, X. Cao, H. Luo, H. Zhu, P. Ghosh, W. Shen, M. Qui, *Laser Photonics Rev.* **2020**, *14*, 1900162.
[30] H. A. Sabea, L. Norel, O. Galangau, T. Roisnel, O. Maury, F. Riobe, S. Rigaut, *Adv. Funct. Mater.* **2020**, *30*, 2002943.
[31] Y. J. Yoo, J. H. Lim, G. J. Lee, K.-I. Jang, Y. M. Song, *Nanoscale* **2017**, *9*, 2986.
[32] J. H. Ko, Y. J. Yoo, Y. J. Kim, S.-S. Lee, Y. M. Song, *Adv. Funct. Mater.* **2020**, *30*, 1908592.
[33] C. Jung, Y. Yang, J. Jang, T. Badloe, T. Lee, J. Mun, S. Moon, J. Rho, *Nanophotonics* **2021**, *10*, 919.
[34] J. Jang, H. Jeong, G. Hu, C.-W. Qiu, K. T. Nam, J. Rho, *Adv. Opt. Mater.* **2019**, *7*, 1970016.
[35] Y. Ma, Y. Dong, S. Liu, P. She, J. Lu, S. Liu, W. Huang, Q. Zhao, *Adv. Opt. Mater.* **2020**, *8*, 1901687.
[36] X. Li, H. Chen, A. M. Kirillov, Y. Xie, C. Shan, B. Wang, C. Shi, Y. Tang, *Inorg. Chem. Front.* **2016**, *3*, 1014.
[37] S. J. Kwon, G. Y. Lee, K. Jung, H. S. Jang, J.-S. Park, H. Ju, I. K. Han, H. Ko, *Adv. Mater.* **2016**, *28*, 7899.
[38] D. Sikdar, J. B. Pendry, A. A. Kornyshev, *Light: Sci. Appl.* **2020**, *9*, 122.
[39] J. Deng, L. Deng, Z. Guan, J. Tao, G. Li, Z. Li, Z. Li, S. Yu, G. Zheng, *Nano Lett.* **2020**, *20*, 1830.
[40] S. Song, X. Ma, M. Pu, X. Li, K. Liu, P. Gao, Z. Zhao, Y. Wang, C. Wang, X. Luo, *Adv. Opt. Mater.* **2017**, *5*, 1600829.
[41] D. H. Kim, Y. J. Yoo, J. H. Ko, Y. J. Kim, Y. M. Song, *Opt. Mater. Express* **2019**, *9*, 8.
[42] Y. J. Kim, Y. J. Yoo, G. J. Lee, D. E. Yoo, D. W. Lee, V. Siva, H. Song, I. S. Kang, Y. M. Song, *ACS Appl. Mater. Interfaces* **2019**, *11*, 11849.
[43] Q. Zhou, J. G. Park, J. Bae, D. Ha, J. Park, K. Song, T. Kim, *Adv. Mater.* **2020**, *32*, 2001467.
[44] R. J. H. Ng, R. V. Krishnan, Z. Dong, J. Ho, H. Liu, Q. Ruan, K. L. Pey, J. K. W. Yang, *Opt. Mater. Express* **2019**, *9*, 788.
[45] M. Song, Z. A. Kudyshev, H. Yu, A. Boltasseva, V. M. Shalaev, A. V. Kildishev, *Opt. Mater. Express* **2019**, *9*, 779.
[46] S. Modak, A. Safaei, D. Chanda, *arXiv:1710.00392*, **2017**, https://arxiv.org/abs/1710.00392
[47] M. A. Kats, F. Capasso, *Laser Photonics Rev.* **2016**, *10*, 5, 735.
[48] H.-C. Wang, C. H. Chu, P. C. Wu, H.-H. Hsiao, H. J. Wu, J.-W. Chen, W. H. Lee, Y.-C. Lai, Y.-W. Huang, M. L. Tseng, S.-W. Chang, D. P. Tsai, *Small* **2018**, *14*, 1703920.
[49] K. D. Vora, A. S. Holland, M. K. Ghantasala, A. Mitchell, *Proc. SPIE* **2004**, *5276*, 162.
[50] N. Ohta, A. Robertson, *Colorimetry: Fundamentals and Applications*, John Wiley and Sons, Hoboken, NJ **2006**.

© 2021 Wiley-VCH GmbH